Quantifying horizontal and vertical movements in Ho Chi Minh city by Sentinel-1 radar interferometry

Dinh HO TONG MINH, Yen-Nhi NGO, Thu Trang LÊ, Trung Chon LE, Hong Son BUI, Quoc Viet VUONG, Thuy LE TOAN

***Abstract*—Ho Chi Minh City (HCMC), the most crowded city and economic hub of Viet Nam, has been experiencing land subsidence over the past decades. This effort aims to contribute the spatial distribution of subsidence in HCMC in its horizontal and vertical components using synthetic aperture radar interferometry (InSAR) time series. To this purpose, an advanced Persistent Scatterers and Distributed Scatterers (PSDS) InSAR technique was applied to two European Space Agency (ESA) Sentinel-1 datasets consisting of 96 ascending and 202 descending images, acquired from 2014 to 2020 over the HCMC area. A time series of 33 COSMO-SkyMed ascending images was also used for comparison. The combination of ascending and descending satellite passes is used to decompose the light of sight velocities into horizontal east-west and vertical components. Taking into account the presence of east-west horizontal motion, our findings indicate that the accuracy of the decomposed vertical velocity can be improved by up to 3 mm/year for Sentinel-1 data. The obtained results revealed that subsidence is most pronounced in the areas along the Sai Gon River, in the northwest-southeast axis, and in the southwest of the city, with a maximum value of 80 mm/yr, which is in accordance with the findings of the literature. The amplitude of east-west horizontal velocities is relatively small and large-scale eastward movement can be observed in the west of the city at a rate of 3-5 mm/yr. This confirmed that the displacement in Ho Chi Minh City area is mainly vertical downward. The obtained velocities are freely available for download from Zenodo. Together, these results reinforced the remarkable suitability of ESA's SAR Sentinel-1 for subsidence applications, even for non-European countries such as Vietnam and Southeast Asia.**

***Index Terms*—Horizontal East-west velocity, LOS, vertical velocity, InSAR time series, Big Data, PSDS, TomoSAR platform, Sentinel-1, Ho Chi Minh City**

I. Introduction

OVER the last 20 years, the population of Ho Chi Minh City (HCMC) has nearly doubled to 9 million people [1], establishing the city as one of the most rapid growing economic centers in Asia [2]. However, subsiding land, rising sea levels, and extensive water facilities based on the delta are bringing about concerns due to global climate change [3]. In this context, monitoring the geographical area of subsidence is essential to mitigate related risks, as it can potentially affect the human population, infrastructure, and buildings.

Since the 2000's, SAR interferometry (InSAR) time series techniques have been employed to accurately map wide-area subsidence from the space ([4], [5], [6], [7], [8]). Particularly, the recently advanced PSDS (persistent scatterers and distributed scatterers) approach is taking over as the primary InSAR tool for many deformation implementations due to its superior performance ([9], [10]). Radar interferometric measurement can only detect millimeter motion in the direction connecting the SAR sensor and the detected area (so-called the line of sight - LOS) [11]. InSAR measurements therefore have a challenge of both interpretation and communication [12]. To deal with this challenge, there is a commonly held assumption about neglecting the motions of the horizontal component when projecting the LOS metric in the vertical direction ([13], [12]). It is possible to separate the LOS into horizontal and vertical derivatives in some regions of interest where two LOS acquisitions are available (e.g., from ascending and descending satellite orbits) ([12], [13], [14]). Unfortunately, this is not the situation in Vietnam and in many non-European countries. Up to now, no precise information is available concerning the decomposed horizontal and vertical motions from InSAR measurements in Vietnam.

In Vietnam, the InSAR method is used extensively in deformation studies using X-band ([15], [16], [17]), C-band ([18], [19]) and L-band ([20], [21], [3]). In particular, in [3], the authors reported a detailed subsidence map that focused on urban areas in the Ho Chi Minh City area for the period 2006-2010 using ALOS PAlSAR data in L-band. It was reported that subsidence zones are serious along the Sai Gon River and in the southwestern part of the city where subsubsurface soils are dominantly Holocene loams. However, the study estimated vertical subsidence using the conventional assumption of projecting the LOS measurement. Fortunately, since 2014, the European Space Agency (ESA) Sentinel-1 constellation has been providing worldwide, open access SAR data with LOS measurements with over 10 TB and over 4700 products per day ([22], [23]). The regularly acquired SAR

Dinh HO TONG MINH is with UMR TETIS, INRAE, University of Montpellier, 500 Rue Jean Francois Breton, 34000 Montpellier, France, e-mail: dinh.ho-tong-minh@inrae.fr.

Yen-Nhi NGO is an independent researcher, 34090 Montpellier, e-mail: ngoyennhi.ho@gmail.com.

Thu Trang LÊ is with CESBIO and Department of Photogrammetry and Remote Sensing, Hanoi University of Mining and Geology, 18 Vien Street, 11910 Hanoi, Vietnam, e-mail: lethutrang@humg.edu.vn.

Trung Chon LE is with Ho Chi Minh City University of Technology, VNU-HCM, 268 Ly Thuong Kiet Street, 70000 Ho Chi Minh City, Vietnam, e-mail: ltchon@hcmut.edu.vn.

Hong Son BUI is with CIREN, DONRE Ho Chi Minh City, 70000 Ho Chi Minh City, Viennam, e-mail: son.ciren@gmail.com

Quoc Viet VUONG is with BK04, 70000 Ho Chi Minh City, Vietnam, e-mail: quoc.viets@yahoo.com.

Thuy LE TOAN is with CESBIO, Toulouse, France, e-mail: thuy.letoan@cesbio.cnes.fr.

images from such satellite mission with a short repeat cycle (e.g., 6 days over Europe and 12 days for the rest of the world) and a large swath width of 250 km on the ground open new capabilities for monitoring the Earth's surface. For example, to cover the HCMC from 2014 to 2020, there are over 200 images in descending and 100 images in ascending passes, respectively. Thus, Sentinel-1 offers the best chance to quantify the horizontal and vertical movements.

Recently, there is a work on the Ho Chi Minh city area carried out by Duffy et al., 2020 [24]. However, the atmospheric mitigation and phase unwrapping did not take into account during the processing. This is because the authors only used Persistent Scatterers Interferometry (PSI) analysis provided by StaMPS from step 1 to step 7 [25]. To our knowledge, StaMPS does not support phase unwrapping correction for PSI approach. To correct such error, either Small Baseline or Multi Temporal Interferometry (or PSDS) approaches in StaMPS is required during step 6 [26]. Furthermore, StaMPS supports atmospheric mitigation in step 8 and step 9. These two factors make the limited results in [24]. For example, we can not find subsidence patterns in the southwest of the city (i.e., District 8). In this paper, we exploit the state-of-the-art PSDS approach for atmospheric mitigation and avoiding phase unwrapping errors, resulting in a better understanding of the capabilities of Sentinel-1 C-band in estimating decomposed horizontal and vertical components for subsidence phenomena in Ho Chi Minh city.

We experimentally show that by taking into account the presence of the horizontal East-west movement, the precision of the decomposed vertical velocity can be improved up to 3 mm/year for Sentinel-1 data. Different from [24], the obtained result reveals that the subsidence pattern in the southwest of the city is similar for three SAR datasets and particularly consistent with findings in [3].

This paper is organized as follows: the study site and SAR data are shown in Section II; the PSDS InSAR algorithm and the combination of two satellite passes are presented in Section III; the results are examined in Section IV; the discussion is provided in Section V; and finally, conclusions are drawn in Section VI.

II. Materials

A. Study site

The study area is the whole area of Ho Chi Minh City, in the southeast of Vietnam. The population exceeds 9 million (in 2019), which is a major contributor to the developments of the country. It is positioned at 106.65 E longitude and 10.85 N latitude. The city is encircled by the Sai Gon River system. The entire study area is about 90 km x 70 km, including the HCMC area and its neighborhoods, see figure 1. The city is comprised of three zones based on their urban growths: (1) the core, where urbanization is accomplished; (2) the fringe, where urban growth is in progress; and (3) the suburban zone for the remaining part of the city. For more details on the study site, the reader can refer to [3].

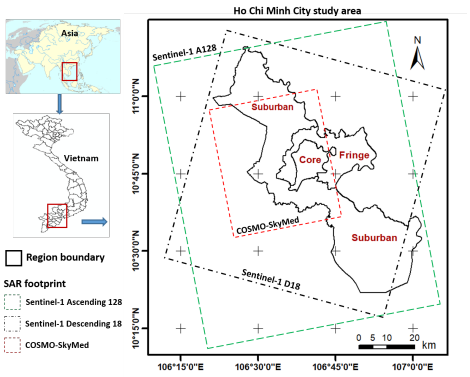

Figure 1. The region of interest is the whole Ho Chi Minh city area coveraged about 90 km x 70 km.

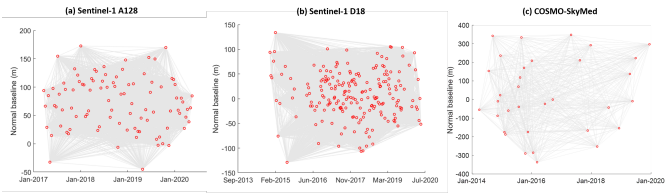

Figure 2. The densed interferometric network in the PSDS technique. (a) Sentinel-1 A128. (b) Sentinel-1 D18. (c) COSMO-SkyMed.

B. SAR data

The SAR stacks are consisting of C-band Sentinel-1 ($\sim$ 5.55 cm) and X-band COSMO-SkyMed ($\sim$ 3.13 cm) data. Their selected footprints are shown in Figure 1. For Sentinel-1 data, both ascending pass track 128 (Sentinel-1 A128) and descending pass track 18 (Sentinel-1 D18) are considered. They are imaged in interferometric mode (i.e., TOPS - Terrain Observation by Progressive Scans [27]), whereas ascending COSMO-SkyMed stack is imaged in stripmap mode. In each stack, each Single Look Complex (SLC) image was coregistered and interpolated on a reference grid. For Sentinel-1 data, we downloaded all SLC images in our region of interest from https://scihub.copernicus.eu. It is worth noting that the ascending Sentinel-1 pass track 128 (Sentinel-1 A128) data is only available from March 2017 from the Sentinel-1A, resulting in 96 images. The COSMO-SkyMed data were selected with a small baseline constraint (i.e., less than 350 m) for interferometric applications and they were provided by the Italian Space Agency under the pilot project COSMO-SkyMed-Open ID226, resulting in 33 images. The characteristic's three datasets is reported in Table I and Figure 2 for the detailed information.

For the Sentinel-1 TOPS mode, coregistration is accomplished using 6 bursts of swath 1 for tracks A128 and D18. These bursts are then merged and cropped to generate stacks of coregistered SLC datasets, as shown in Figure 1. The subset operator is not performed on the COSMO-SkyMed scenes in order to maximize their coverages. Although we exploit all possible information in the PSDS technique, as described in III-A, we selected the COSMO-SkyMed reference date in the middle of the geometric baseline distribution to minimize

Table I
CHARACTERISTICS OF SAR DATA.

SAR sensor	Total image	Range-Azimuth (m)	Start date	Reference date	End date
Sentinel-1 A128	96	2.3 - 14.0	Mar. 20, 2017	30 Sept. 2019	May 15, 2020
Sentinel-1 D18	202	2.3 - 14.0	Nov. 23, 2014	27 Sept. 2018	May 31, 2020
COSMO-SkyMed	33	1.0 - 2.3	Mar. 30, 2014	15 Sept. 2016	Dec. 13, 2019

registration errors due to long baselines. For Sentinel-1, the baseline tube is relatively small, but the coregistration was carefully handled to avoid a phase jump in the azimuthal direction [28]. In detail, in the azimuth direction, the accuracy of a few per-mille of a pixel is required. To meet this accuracy, we exploited spectral diversity information which considers the interferometric phase of the burst overlap regions [29]. The final constant offset will be corrected for 6 bursts.

III. METHOD

The advantage of the InSAR time series approach is to minimize decorrelation problems in order to estimate ground deformations in a robust manner ([4], [30]). Let us suppose that N SLC SAR images are available for our region of interest. These images are then resampled on a common/reference grid. We further suppose that the contributions of orbit and topography have been compensated in the these phases. The differential residual phase φ^n can be composed of the phase contributions related to residual topography, deformation, atmosphere, and noise [11]:

$$\varphi^n = W\left\{\varphi^n_{topo} + \varphi^n_{defo} + \varphi^n_{aps} + \varphi^n_{noise}\right\} \quad (1)$$

where W is the wrapping operator; $\varphi^n_{topo} = \frac{4\pi b_n}{\lambda sin\theta R_n}\varepsilon^z$ is the phase related to residual topography; φ^n_{defo} is the deformation phase; φ^n_{aps} is the phase due to atmospheric screen, which can be the signal delay due to weather conditions; and φ^n_{noise} is the noise due to all possible factors such as mis-coregistration, temporal decorrelation, spatial decorrelation, orbit, soil moisture, and thermal noise. ε^z is the elevation error; b_n is the normal baseline relative to the n-th image with respect to the reference image; θ is the local incidence angle; λ is the radar wavelength; R_n is the LOS distance between the target and the n-th orbit acquisition.

It is usefully to split the deformation phase into two components:

$$\varphi^n_{defo} = \frac{4\pi}{\lambda}d_n = \frac{4\pi t_n}{\lambda}v_p + \mu_{NL} \quad (2)$$

where d_n is the LOS distance change of the target; v is the constant velocity; t_n is the temporal baseline; and μ_{NL} is the phase term due to a possible non-linear motion. In Figure 3, an example of target motion between the n-th and reference acquisition time is shown.

Our problem is to estimate the deformed phase from equation 1 using $N-1$ differential interferograms. Specifically, we have a nonlinear system of $N-1$ equations and two parameters of interest ε^z and v. The interferometric phase is naturally given as a wrapped number and needs to be unwrapped (i.e., by adding a certain integer ambiguity number 2π [31]) to obtain ε^z and v. In the InSAR literature, there are two strategies to unwrap the equation 1. In the first approach, the interferograms are spatially multilooked, filtered, and unwrapped on Distributed Scatterers (DS) [32]. In this way, the model in equation 1 becomes linear and the inversion is straightforward by using a Singular Value Decomposition ([32], [33]). In the second approach, the analysis can be carried out on stable point-like pixels using the wrapped phase in model equation 1, avoiding the introduction of the unwrapping error. Such stable targets are named Permanent/persistent Scatter (PS) ([4], [30], [5]). In practice, the relative ε^z and v for every PS pair are jointly estimated by a temporal model maximizing [10]. Recently, the motivation of using both PS and DS is highlighted, in order to optimize the phase estimations ([34], [35], [36], [37], [9]).

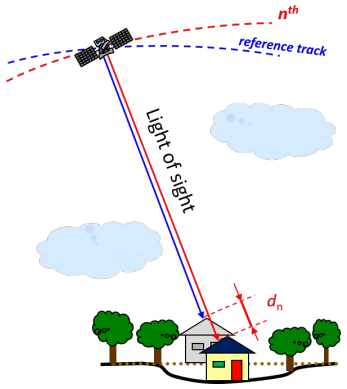

Figure 3. A schematic example of line of sight target motion captured by InSAR technique.

A. The PSDS technique

The principle idea of the PSDS technique is to enhance signal-to-noise ratio (SNR) of DS so that it can emulate PS. To do it, it is often employed a phase linking technique ([38]) to extract the best estimates $N-1$ DS interferometric phases from all the $N(N-1)/2$ interferometric phases available of N images ([34], [35], [36], [9]). For this purpose, to select a good DS candidate, it is required to define a brotherhood. This is characterized by a similarly statistical homogeneous pixels (SHP) test. A traditional two-sample test (i.e., Kolmogorov-Smirnov [9]) can be used. Whenever the SHP family is available, a DS sample coherence matrix ($\hat{\Gamma}$) (i.e, which by definition contains $N(N-1)/2$ phase values) can be generated for estimating $N-1$ linked phase ($\hat{\boldsymbol{\lambda}}$):

$$\hat{\boldsymbol{\lambda}} = argmax_{\lambda}\left\{\Lambda^H\left(|\hat{\Gamma}|^{-1}\circ\hat{\Gamma}\right)\Lambda\right\} \quad (3)$$

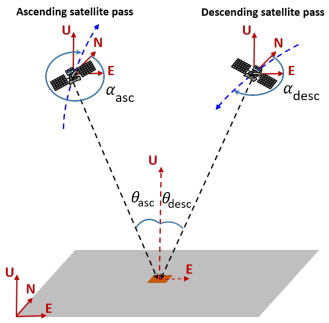

Figure 4. A schematic view of the InSAR geometry for line of sight directions on ascending and descending observations.

where $\Lambda = exp(j\boldsymbol{\lambda})$; ^{H} is Hermitian conjugation; and $\circ$ indicates the Hadamard entry-wise product. After this procedure, the DS can emulate PS. The rest of PSDS technique will be carried out as the traditional PSI. For more details on the technique, the reader can be found in [10].

In this work, we use the TomoSAR platform to carry out PSDS processing as demonstrated in [3], [19], [17] with an update on using Baumgartner-Weiss-Schindler test statistic for DS candidate selections [39]. As supported in [40], two-sample test based on the Baumgartner-Weiss-Schindler statistic is more robust than traditional Kolmogorov-Smirnov [9] and Anderson-Darling tests [41].

B. The combination of ascending and descending satellite passes

By combining both ascending and descending information (see Figure 4), we can decompose the LOS velocities into horizontal East-west and vertical components as follow [12]:

$$v_{los} = [sin\theta\, cos\alpha \quad -sin\theta\, sin\alpha \quad -cos\theta] \begin{bmatrix} v_E \\ v_N \\ v_U \end{bmatrix} \tag{4}$$

where v_{los} is the LOS velocity, α is the azimuth heading vector, and v_E, v_N, v_U are the East, North, and vertical motion components, respectively. The equation 4 has three unknowns but we have only two observational constraints from ascending and descending LOS measurements. We add the additional constraint to the equation 4 where the North-south motion is assumed to be zero. For this purpose, both ascending and descending velocity measurements are resampled to a common grid with a 50 m spatial resolution. We note that there is no spatial interpolation performed at the grid where PSDS measure points are not available. Finally, by using the equation 6.5 in [36], we can estimate the standard deviation of velocity at 0.35 mm/year and 0.10 mm/year for our Sentinel-1 A128 and D18 dataset, respectively. Although the difference is small, we also take it into account for a weighted combination.

IV. Results

A. Surface subsidence

The Sentinel-1 A128, Sentinel-1 D128, and COSMO-SkyMed data were treated by using PSDS processing. In this section, to have the same metric for comparison among velocity's results, LOS measurements are projected to vertical direction by dividing the cosine of the incidence angle (i.e., neglecting the presence of horizontal motions). The reference point was set at the same location in a stable area in District 1 (i.e., 10.782°N and 106.698°E), as suggested in [3]. The result was plotted in Figure 5, reflecting similar subsidence patterns. Subsidence is severe and very visible in areas along the river and the southwest of the city, consistent with findings reported in [3].

To make it comparable among three velocities, a zoom focused on a red-bordered rectangle area (see Figure 5c) is shown in Figure 6a, b and c. More than 35000, 29000, and 87000 PSDS measuring points in Sentinel-1 A128, Sentinel-1 D18, and COSMO-SkyMed datasets, respectively, were identified within an area of about 42 km^2. The lower measurement points in Sentinel-1 is expected due to the higher spatial resolution of COSMO-SkyMed (see Table I).

A buffer of 100 m diameter centered on a certain line AB in Figure 6c was associated with a PSDS cluster. All the PSDS points inside the 300 m bin cluster were used to calculate the average velocity for each dataset. The profile was plotted in Figure 6d. It is noted that the maximum rate is up to -80 mm/year, representing a highly vulnerable area.

Finally, to appreciate our long term datasets, a time series plot is reported in Figure 6e. Two Sentinel-1 datasets are referred to the same starting temporal reference in COSMO-SkyMed (i.e., 30 March 2014). The displacement history at two points representing moderate (P_1) and severe (P_2) subsidence is highlighted. It is clear that subsidence is primarily linear, which agrees well with findings presented in [3].

B. East-west and vertical velocities

The ascending and descending velocities (see Figure 5) can provide a detailed picture of Ho Chi Minh city area subsidence. However, it maybe some of ambiguities associated with LOS measurements due to non-negligable influences of horizontal displacement. To remove it, we decompose the LOS velocities into East-west and vertical components using Equation 4. The decomposed horizontal East-west and vertical velocities are reported in Figure 7. We note that the decomposed products are only available at common spatial areas from both A128 and D18 geometries. To facilitate visualization of the subsidence results, Figure 8 is highlighted in a severe area in the south of the city (e.g., District 8 and 7). It is expected to observe that there is no significant difference in Figure 7a with respect to Figure 5 as active tectonics are not found in southern Vietnam [42].

The resulting decomposed East-west velocity is more difficult to interpret than the vertical component. It is evident that the magnitude of east-west components is relatively small with

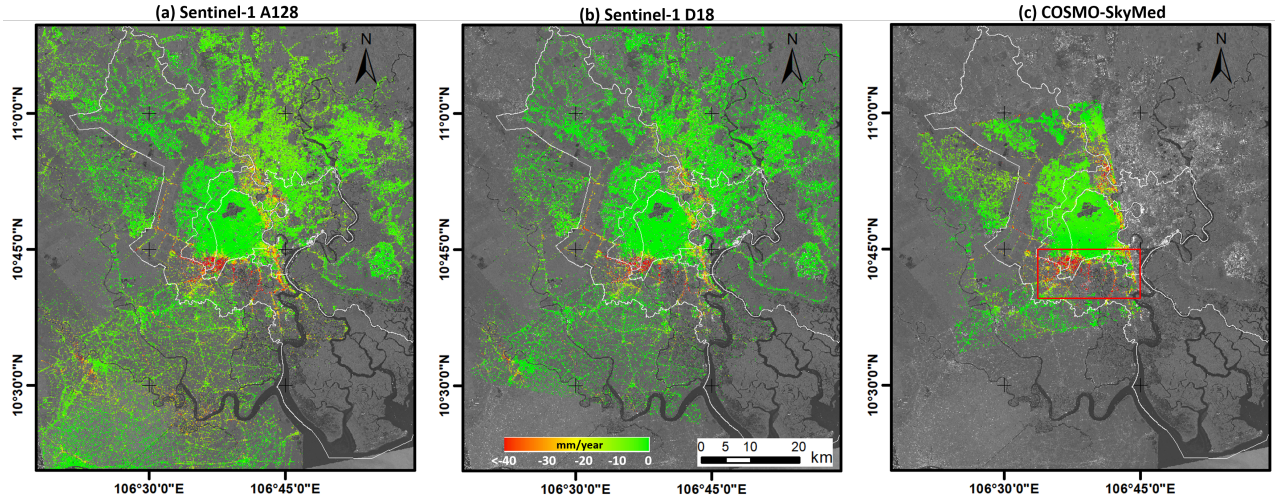

Figure 5. Vertical velocities by projecting of LOS measurements into the vertical direction. Subsidence is coded by red colors. (a) Sentinel-1 A128. (b) Sentinel-1 D18. (c) COSMO-SkyMed.

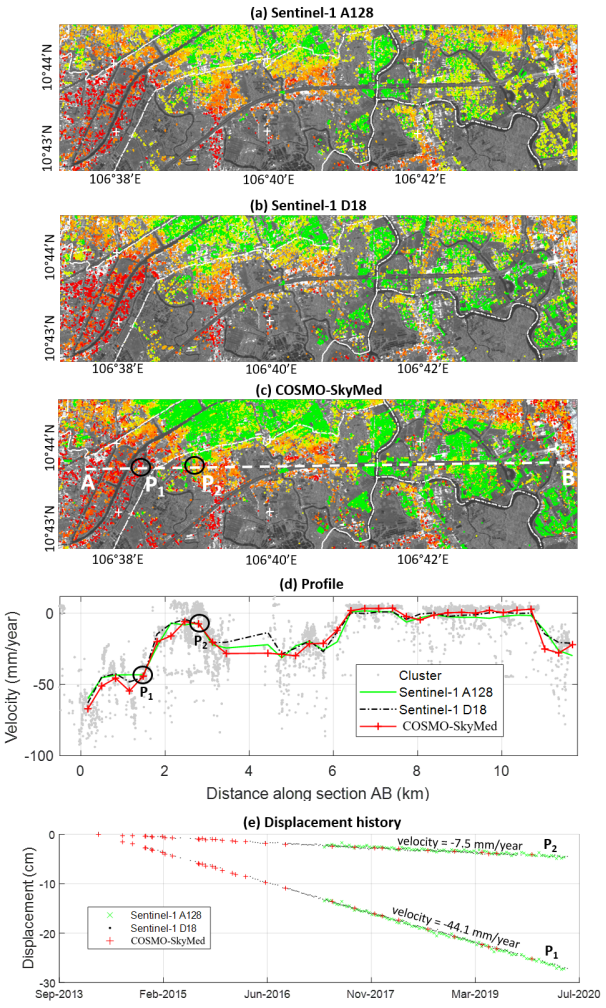

Figure 6. The velocity, profile, and displacement history in a red-bordered rectangle in Figure 5c. The small area is coveraged about 3.5 km x 12 km. In (a), (b), and (c), a zoom version of velocity map. (d) Velocity cross section along point A and B. (e) An example displacement history at points P_1 and P_2. The color reference in (a), (b), and (c) is the same in Figure 5.

respect to vertical contributions. It means that there is mainly vertical downward displacement happened in HCMC areas. The most prominent feature in East-west velocity is the large-scale eastward motion in the west of the city at a rate of 3-5 mm/year. By using the standard deviation of LOS velocity at 0.35 mm/year and 0.1 mm/year for the A128 and D18 tracks, respectively (see Section III-B), we can estimate the standard deviation of the horizontal East-west motion at $\sim$ 0.65 mm/year.

To quantify the relationship between horizontal and vertical motions, we plotted their joint distribution and the associated standard deviation in Figure 9. The maximum magnitude of East-west velocity is about 10 mm/year. The joint distribution is normalized between 0 and 1 to better do the interpretation. It is evident that they are independent random variables (i.e., correlation coefficient $R^2 = 10^{-3}$). For vertical velocities varying from -40 mm/year to zero, we can observe that the mean of East-west velocity is approximately close to zero, whereas its standard deviation is decreased from 4.5 mm/year to 0.9 mm/year.

C. Comparison vertical velocities

The impact of horizontal motion on the projection of LOS measurements into the vertical direction is investigated in this section. To do it, all measurements (see Figure 5) were resampled to a common grid with a 50 m spatial resolution as the decomposed vertical velocity product (see Figure 7a). A total of 101620 50-m pixels is found for the same area of interest between Sentinel-1 and COSMO-SkyMed data. The pixel-wise joint distributions between decomposed and projected vertical results were shown in Figure 10. The distribution is normalized between 0 and 1 to facilitate visualization. Strong correlation coefficients (i.e., correlation coefficient $R^2 \geq 0.67$ for 101620 samples) were found. The Root Mean Square Difference is from 2.9 mm/year to 3.1 mm/year for Sentinel-1 and 3.9 mm/year for COSMO-SkyMed.

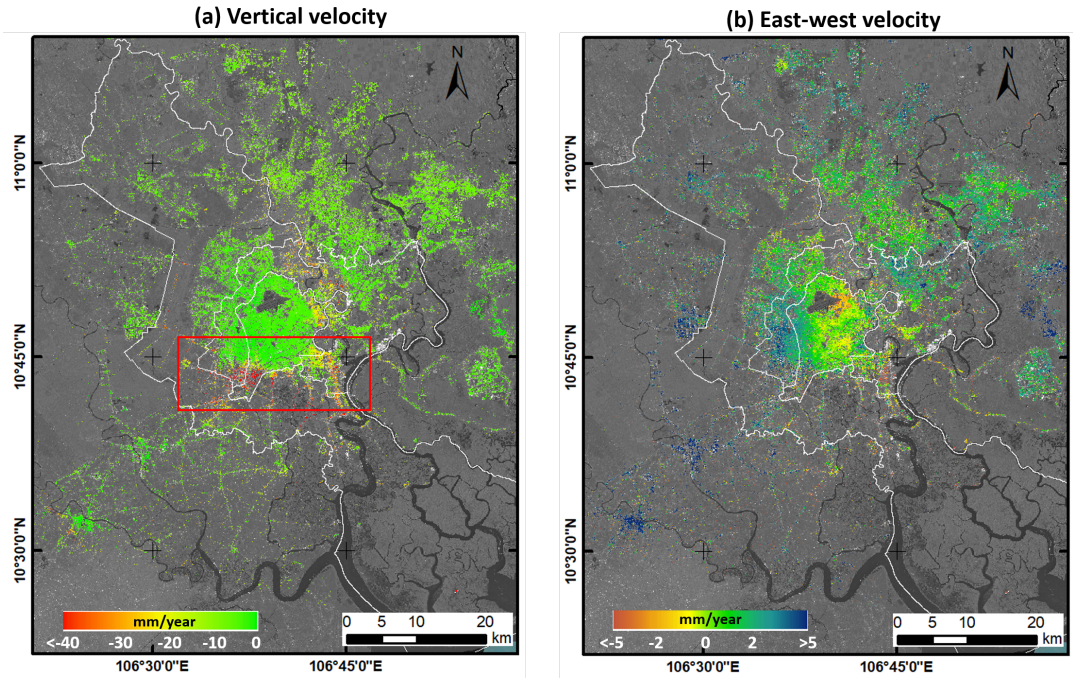

Figure 7. Vertical and horizontal East-west velocities based on Sentinel-1 descending and ascending passes. (a) Vertical velocity, negative velocities (red colors) represent movement subsidence. (b) Horizontal East-west velocity, positive velocities (blue colors) represent movement Eastward.

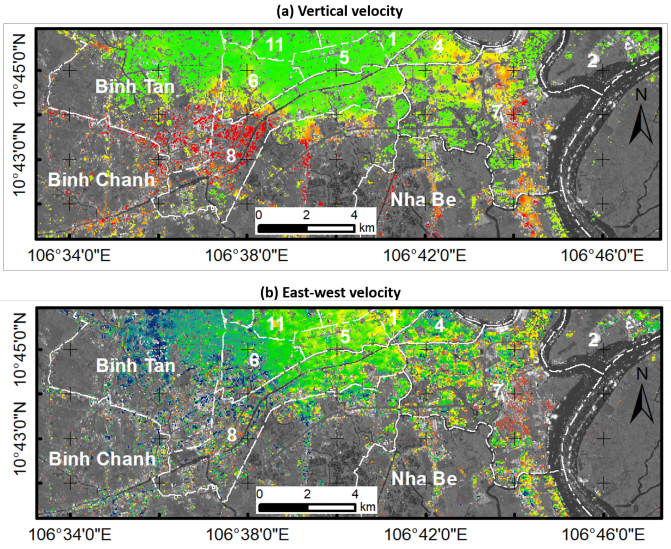

Figure 8. A zoom version in a red-bordered rectangle in Figure 7a. (a) Vertical velocity. (b) Horizontal East-west velocity. The color reference in (a) and (b) is the same in Figure 7. White labels indicate district names.

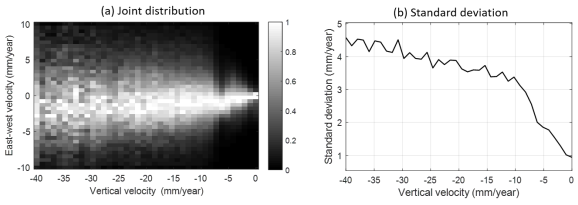

Figure 9. The relation between horizontal East-west movement and vertical surface velocity from Sentinel-1 data. (a) The joint distribution. (b) The standard deviation.

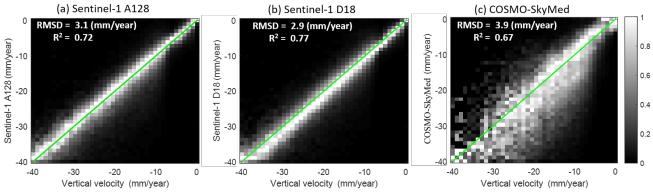

Figure 10. The joint distribution between decomposed vertical and projected vertical velocities, with correlation coefficient (R^2) and Root Mean Square Difference (RMSD). (a) Sentinel-1 A128. (b) Sentinel-1 D18. (c) COSMO-SkyMed.

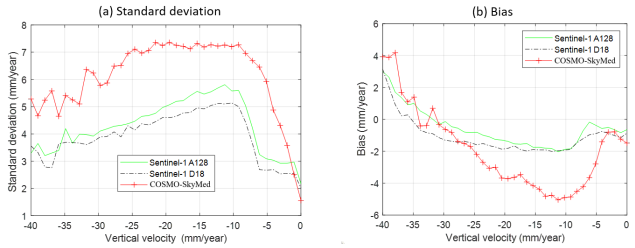

Figure 11. Comparison vertical velocities between projected and decomposed products for Sentinel-1 A128, Sentinel-1 D18, and COSMO-SkyMed. (a) The standard deviation. (b) The bias.

To quantify the detail of the magnitude of error, the standard deviation and bias were calculated and reported in Figure 9. The results of projecting LOS to vertical would erroneously indicate that the bias value of ± 2 mm/year and ± 4 mm/year can be made for Sentinel-1 and COSMO-SkyMed datasets, respectively.

V. Discussion

First of all, this is the first work (to our knowledge) using data from ascending and descending measurements to provide decomposed horizontal East-west and vertical velocities in the Vietnam area using the advanced PSDS InSAR technique technique. This is not possible for many non-Europe countries before ESA's Sentinel-1 era. In fact, there is limited ESA SAR data (e.g., C-band ERS-1/2 and ENVISAT ASAR) exist that can be used for InSAR time series techniques. This is the reason why previous studies are based on L-band from Japan Aerospace Exploration Agency ALOS PALSAR ([20], [3]) and X-band (e.g., COSMO-SkyMed from Italian Space Agency and TerraSAR-X from German Space Agency) ([16], [17]). They were all based on the assumption of neglecting the presence of horizontal motions, projecting LOS measurements into the vertical values.

It is important to point out that our subsidence results were analyzed only on pixels where their time series signals are stable or high signal-to-noise ratio (see Section III). It does not mean the deformation does not happen at other pixels. For example, although we mapped subsidence for the whole city area, there is an area that strongly lacks PSDS points in the Southeast part (see Figure 5), which is mainly Can Gio mangrove forest's area. This is clearly due to temporal decorrelation caused by vegetation ([43], [44], [45]). Future longer wavelength missions such as NISAR L-band [46], Tandem-L [47], ROSE L-band [48], and BIOMASS P-band ([49], [50]) are expected to yield better performances in vegetation areas due to minimizing temporal decorrelation.

To provide an independent measurement for comparison, we exploited COSMO-SkyMed X-band SAR data as shown in Figures 5c, 6, 10c, and 11. It is worth pointing out that this stack is characterized by higher spatial resolution and shorter wavelength (see Table I). Consequently, denser pixels were identified (i.e., 87000 pixels vs 29000-35000 pixels from Sentinel-1 data, see Section IV-A). This is the reason why the RMSD, standard deviation, and bias of projected COSMO-SkyMed results are slightly bigger than the projected Sentinel-1 A128 and D18 measurements. In other words, it does not mean COSMO-SkyMed data is of minority quality to Sentinel-1. In fact, with X-band (e.g., COSMO-SkyMed and TerraSAR-X), it is possible to study at a target-scale level such as bridges and buildings [51]. Particularly, Ho Tong Minh et al., [17] have demonstrated the feasibility of subsidence estimates by X-band InSAR even in conditions impacted by a strong atmosphere in northern Vietnam, reinforcing the scientific potential for a new Vietnamese X-band SAR space-borne mission (JV-LOTUSat).

It is worth pointing out that there is a recent work on the same site carried out by Duffy et al., 2020 [24]. However, an independent measurement for comparison results was missed and there was no horizontal motion reported. In our contributions, we provided COSMO-SkyMed (i.e., 101620 50-m pixels) for independent comparison. We also reported horizontal motion and demonstrated its added value to vertical motion estimation. Finally, different from [24], we found that the subsidence pattern in the southwest of the city (i.e., District 8) is similar for three SAR datasets (see Figures 6 and 8a), consistent with findings in [3].

Given ascending and descending SAR data systematically available from Sentinel-1, nowadays, neglecting the impact of horizontal motion in converting LOS measurements into the vertical direction is generally not recommended. We have shown that the improvement of 3 mm/year for Sentinel-1 data (see Figure 10a and b) is evident with the combination. However, since only the horizontal East-west and vertical components are estimated, a slight error can be introduced because of neglecting the North-south component. Fortunately, this error is very small (i.e., 0.1 mm/year [13]) in many isotropic deformation cases, whereas it becomes critical for non-isotropic deformation scenarios (e.g., landslide and earthquake deformation phenomena) ([12], [14]). Finally, the Sentinel-1 constellation is the only system that can provide the systematic survey, open-access, and long term SAR data. Therefore, it is recommended for using Sentinel-1 as a SAR data resource for operational subsidence monitoring tasks, particularly for large-scale, delta-wide, and nation-wide coverages.

VI. Conclusions

We have produced, to our knowledge, the first horizontal East-West and vertical motion maps in Ho Chi Minh City area by using the Sentinel-1 PSDS InSAR technique. This is the largest regional measurement reported in Vietnam from a coherent InSAR analysis to date, covering about 5 600 km^2 area. The velocities are freely available for download [52]. The relative comparison with COSMO-SkyMed indicated good agreement with the strong correlation for vertical velocities. The spatial distribution of the vertical velocity reflects similar subsidence patterns with previous studies. Along the Sai Gon river in the Northwest-Southeast axis and the Southwest of the city, subsidence is most severe at a rate up to 80 mm/year. The study shows that the magnitude of horizontal East-West velocities is relatively small, showing the large-scale eastward motion in the west of the city at a rate of 3-5 mm/year. This means the displacement in Ho Chi Minh City area is mainly vertical downward. Together, these results confirm the remarkable suitability of ESA's Sentinel-1 SAR for continuously monitoring ground subsidence applications with the frequent and reliable coverage even for non-Europe countries such as Vietnam and Southeast Asia. Thus, it is recommended to develop operational projects such as delta-wide and national wide initiatives for long term motion monitoring. Consequently, this will foster the developments of downstream solutions by the final beneficiaries: infrastructure managers (e.g. roads, railways, pipelines), civil engineering companies, regional and municipality administrators, and public policymakers.

VII. Acknowledgments

This work was supported in part by the Centre National d'Etudes Spatiales/Terre, Ocean, Surfaces Continentales, Atmosphere (CNES/TOSCA - project MekongInSAR), UMR

TETIS, and Institut national de recherche en agriculture, alimentation et environnement (INRAE). The first author would like to thank the Italian Space Agency for free access data COSMO-SkyMed-Open ID226.

REFERENCES

[1] GSO Vietnam, *Statistical yearbook 2019*. General Statistics Office of Vietnam, 2020.

[2] D. Seo and Y. Kwon, "In-migration and housing choice in ho chi minh city:toward sustainable housing development in vietnam," *Sustainability*, vol. 9, no. 10, p. 1738, sep 2017.

[3] D. Ho Tong Minh, L. Van Trung, and T. L. Toan, "Mapping ground subsidence phenomena in ho chi minh city through the radar interferometry technique using alos palsar data," *Remote Sensing*, vol. 7, no. 7, pp. 8543–8562, 2015. [Online]. Available: https://www.mdpi.com/2072-4292/7/7/8543

[4] A. Ferreti, C. Prati, and F. Rocca, "Nonlinear subsidence rate estimation using permanent scatterers in differential sar interferometry," *IEEE Transactions on Geoscience and Remote Sensing*, vol. 38, no. 5, pp. 2202–2212, 2000.

[5] A. Hooper, H. Zebker, P. Segall, and B. Kampes, "A new method for measuring deformation on volcanoes and other natural terrains using insar persistent scatterers," *Geophysical research letters*, vol. 31, no. 23, 2004.

[6] L. Solari, M. Del Soldato, S. Bianchini, A. Ciampalini, P. Ezquerro, R. Montalti, F. Raspini, and S. Moretti, "From ers 1/2 to sentinel-1: Subsidence monitoring in italy in the last two decades," *Frontiers in Earth Science*, vol. 6, p. 149, 2018. [Online]. Available: https://www.frontiersin.org/article/10.3389/feart.2018.00149

[7] M. Haghshenas Haghighi and M. Motagh, "Ground surface response to continuous compaction of aquifer system in Tehran, Iran: Results from a long-term multi-sensor InSAR analysis," *Remote Sensing of Environment*, vol. 221, pp. 534–550, Feb. 2019.

[8] J. Catalao, D. Raju, and G. Nico, "Insar maps of land subsidence and sea level scenarios to quantify the flood inundation risk in coastal cities: The case of singapore," *Remote Sensing*, vol. 12, no. 2, 2020. [Online]. Available: https://www.mdpi.com/2072-4292/12/2/296

[9] A. Ferretti, A. Fumagalli, F. Novali, C. Prati, F. Rocca, and A. Rucci, "A new algorithm for processing interferometric data-stacks: SqueeSAR," *Geoscience and Remote Sensing, IEEE Transactions on*, vol. 49, no. 9, pp. 3460–3470, Sept 2011.

[10] D. Ho Tong Minh, R. Hanssen, and F. Rocca, "Radar interferometry: 20 years of development in time series techniques and future perspectives," *Remote Sensing*, vol. 12, no. 9, 2020. [Online]. Available: https://www.mdpi.com/2072-4292/12/9/1364

[11] R. F. Hanssen, *Radar Interferometry: Data Interpretation and Error Analysis*. Dordrecht: Kluwer Academic Publishers, 2001. [Online]. Available: http://www.amazon.com/exec/obidos/tg/stores/detail/-/books/0792369459/glance/ref=dpr_sdp_bb/102-6255647-1210555

[12] T. J. Wright, B. E. Parsons, and Z. Lu, "Toward mapping surface deformation in three dimensions using insar," *Geophysical Research Letters*, vol. 31, no. 1, 2004. [Online]. Available: https://agupubs.onlinelibrary.wiley.com/doi/abs/10.1029/2003GL018827

[13] T. Fuhrmann and M. C. Garthwaite, "Resolving three-dimensional surface motion with insar: Constraints from multi-geometry data fusion," *Remote Sensing*, vol. 11, no. 3, 2019. [Online]. Available: https://www.mdpi.com/2072-4292/11/3/241

[14] J. R. Weiss, R. J. Walters, Y. Morishita, T. J. Wright, M. Lazecky, H. Wang, E. Hussain, A. J. Hooper, J. R. Elliott, C. Rollins, C. Yu, P. J. González, K. Spaans, Z. Li, and B. Parsons, "High-resolution surface velocities and strain for anatolia from sentinel-1 insar and gnss data," *Geophysical Research Letters*, vol. 47, no. 17, p. e2020GL087376, 2020, e2020GL087376 2020GL087376. [Online]. Available: https://agupubs.onlinelibrary.wiley.com/doi/abs/10.1029/2020GL087376

[15] T. Q. Cuong, D. Ho Tong Minh, L. Van Trung, and T. Le Toan, "Ground subsidence monitoring in vietnam by multi-temporal insar technique," in *2015 IEEE International Geoscience and Remote Sensing Symposium (IGARSS)*, 2015, pp. 3540–3543.

[16] T. S. Le, C.-P. Chang, X. T. Nguyen, and A. Yhokha, "Terrasar-x data for high-precision land subsidence monitoring: A case study in the historical centre of hanoi, vietnam," *Remote Sensing*, vol. 8, no. 4, 2016. [Online]. Available: https://www.mdpi.com/2072-4292/8/4/338

[17] D. Ho Tong Minh, Q. C. Tran, Q. N. Pham, T. T. Dang, D. A. Nguyen, I. El-Moussawi, and T. Le Toan, "Measuring ground subsidence in ha noi through the radar interferometry technique using terrasar-x and cosmos skymed data," *IEEE Journal of Selected Topics in Applied Earth Observations and Remote Sensing*, vol. 12, no. 10, pp. 3874–3884, Oct 2019.

[18] D. Ho Tong Minh, Q. V. Vuong, V. T. Le, and Y.-N. Ngo, "Comparison Stripmap Cosmos SkyMed X-Band and TOPS Sentinel-1C Band in Estimating Ground Subsidence Using Irstea TomoSAR Platform: Ho Chi Minh City Case Study," in *Living Planet Symposium*, ser. ESA Special Publication, vol. 740, august 2016, p. 73.

[19] D. Ho Tong Minh and Y.-N. Ngo, "Tomosar platform supports for sentinel-1 tops persistent scatterers interferometry," in *2017 IEEE International Geoscience and Remote Sensing Symposium (IGARSS)*, July 2017, pp. 1680–1683.

[20] V. K. Dang, C. Doubre, C. Weber, N. Gourmelen, and F. Masson, "Recent land subsidence caused by the rapid urban development in the Hanoi region (Vietnam) using ALOS InSAR data," *Natural Hazards and Earth System Sciences*, vol. 14, no. 3, pp. 657–674, Mar. 2014.

[21] L. E. Erban, S. M. Gorelick, and H. A. Zebker, "Groundwater extraction, land subsidence, and sea-level rise in the mekong delta, vietnam," *Environmental Research Letters*, vol. 9, no. 8, p. 084010, aug 2014. [Online]. Available: https://doi.org/10.1088%2F1748-9326%2F9%2F8%2F084010

[22] R. Torres, P. Snoeij, D. Geudtner, D. Bibby, M. Davidson, E. Attema, P. Potin, B. Rommen, N. Floury, M. Brown, I. N. Traver, P. Deghaye, B. Duesmann, B. Rosich, N. Miranda, C. Bruno, M. L'Abbate, R. Croci, A. Pietropaolo, M. Huchler, and F. Rostan, "Gmes sentinel-1 mission," *Remote Sensing of Environment*, vol. 120, pp. 9 – 24, 2012, the Sentinel Missions - New Opportunities for Science. [Online]. Available: http://www.sciencedirect.com/science/article/pii/S0034425712000600

[23] T. Hahmann and E. Diedrich, "Three years of operations of the sentinel-1 and sentinel-3-olci pac at german aerospace center," Mar 2018.

[24] C. E. Duffy, A. Braun, and V. Hochschild, "Surface subsidence in urbanized coastal areas: Psi methods based on sentinel-1 for ho chi minh city," *Remote Sensing*, vol. 12, no. 24, 2020. [Online]. Available: https://www.mdpi.com/2072-4292/12/24/4130

[25] A. Hooper, P. Segall, and H. Zebker, "Persistent scatterer interferometric synthetic aperture radar for crustal deformation analysis, with application to volcán alcedo, galápagos," *Journal of Geophysical Research: Solid Earth*, vol. 112, no. B7, 2007. [Online]. Available: https://agupubs.onlinelibrary.wiley.com/doi/abs/10.1029/2006JB004763

[26] E. Hussain, A. Hooper, T. J. Wright, R. J. Walters, and D. P. S. Bekaert, "Interseismic strain accumulation across the central north anatolian fault from iteratively unwrapped insar measurements," *Journal of Geophysical Research: Solid Earth*, vol. 121, no. 12, pp. 9000–9019, 2016. [Online]. Available: https://agupubs.onlinelibrary.wiley.com/doi/abs/10.1002/2016JB013108

[27] F. De Zan and A. Monti Guarnieri, "Topsar: Terrain observation by progressive scans," *IEEE Transactions on Geoscience and Remote Sensing*, vol. 44, no. 9, pp. 2352–2360, Sep. 2006.

[28] P. Prats-Iraola, R. Scheiber, L. Marotti, S. Wollstadt, and A. Reigber, "Tops interferometry with terrasar-x," *IEEE Transactions on Geoscience and Remote Sensing*, vol. 50, no. 8, pp. 3179–3188, 2012.

[29] R. Scheiber and A. Moreira, "Coregistration of interferometric sar images using spectral diversity," *IEEE Transactions on Geoscience and Remote Sensing*, vol. 38, no. 5, pp. 2179–2191, 2000.

[30] A. Ferretti, C. Prati, and F. Rocca, "Permanent scatterers in sar interferometry," *IEEE Transactions on geoscience and remote sensing*, vol. 39, no. 1, pp. 8–20, 2001.

[31] D. C. Ghiglia and M. D. Pritt, *Two-dimensional phase unwrapping: theory, algorithms, and software*. New York: John Wiley & Sons, Inc, 1998.

[32] P. Berardino, G. Fornaro, R. Lanari, and E. Sansosti, "A new algorithm for surface deformation monitoring based on small baseline differential SAR interferograms," *Geoscience and Remote Sensing, IEEE Transactions on*, vol. 40, no. 11, pp. 2375–2383, 2002.

[33] D. A. Schmidt and R. Bürgmann, "Time-dependent land uplift and subsidence in the santa clara valley, california, from a large interferometric synthetic aperture radar data set," *Journal of Geophysical Research: Solid Earth*, vol. 108, no. B9, 2003.

[34] G. Fornaro, A. Monti Guarnieri, A. Pauciullo, and F. De-Zan, "Maximum liklehood multi-baseline sar interferometry," *IEE Proceedings - Radar, Sonar and Navigation*, vol. 153, no. 3, pp. 279–288, June 2006.

[35] A. Ferretti, F. Novali, F. D. Zan, C. Prati, and F. Rocca, "Moving from ps to slowly decorrelating targets: a prospective view," in *European Conference on Synthetic Aperture Radar*, 2008.

[36] F. Rocca, "Modeling interferogram stacks," *Geoscience and Remote Sensing, IEEE Transactions on*, vol. 45, no. 10, pp. 3289–3299, Oct. 2007.
[37] A. Hooper, "A multi-temporal insar method incorporating both persistent scatterer and small baseline approaches," *Geophys. Res. Lett.*, vol. 35, no. L16302, pp. 1–5, 2008.
[38] A. M. Guarnieri and S. Tebaldini, "On the exploitation of target statistics for SAR interferometry applications," *Geoscience and Remote Sensing, IEEE Transactions on*, vol. 46, no. 11, pp. 3436–3443, Nov. 2008.
[39] M. Neuhäuser, "An exact two-sample test based on the baumgartner-weiss-schindler statistic and a modification of lepage's test," *Communications in Statistics - Theory and Methods*, vol. 29, no. 1, pp. 67–78, 2000. [Online]. Available: https://doi.org/10.1080/03610920008832469
[40] M. Jiang, X. Ding, R. F. Hanssen, R. Malhotra, and L. Chang, "Fast statistically homogeneous pixel selection for covariance matrix estimation for multitemporal insar," *IEEE Transactions on Geoscience and Remote Sensing*, vol. 53, no. 3, pp. 1213–1224, March 2015.
[41] K. Goel and N. Adam, "A distributed scatterer interferometry approach for precision monitoring of known surface deformation phenomena," *IEEE Transactions on Geoscience and Remote Sensing*, vol. 52, no. 9, pp. 5454–5468, Sep. 2014.
[42] C. Lepvrier, N. Van Vuong, H. Maluski, P. Truong Thi, and T. Van Vu, "Indosinian tectonics in vietnam," *Comptes Rendus Geoscience*, vol. 340, no. 2, pp. 94 – 111, 2008, l'orogénèse triasique indosinienne en Asie de l'Est. [Online]. Available: http://www.sciencedirect.com/science/article/pii/S1631071307002969
[43] H. A. Zebker and J. Villasenor, "Decorrelation in interferometric radar echoes," *Geoscience and Remote Sensing, IEEE Transactions on*, vol. 30, no. 5, pp. 950–959, sept 1992.
[44] D. Ho Tong Minh, S. Tebaldini, F. Rocca, and T. Le Toan, "The impact of temporal decorrelation on biomass tomography of tropical forests," *IEEE Geoscience and Remote Sensing Letters*, vol. 12, no. 6, pp. 1297–1301, 2015.
[45] Y. Bai, S. Tebaldini, D. H. T. Minh, and W. Yang, "An empirical study on the impact of changing weather conditions on repeat-pass sar tomography," *IEEE Journal of Selected Topics in Applied Earth Observations and Remote Sensing*, vol. 11, no. 10, pp. 3505–3511, 2018.
[46] P. A. Rosen, Y. Kim, R. Kumar, T. Misra, R. Bhan, and V. R. Sagi, "Global persistent sar sampling with the nasa-isro sar (nisar) mission," in *2017 IEEE Radar Conference (RadarConf)*, May 2017, pp. 0410–0414.
[47] I. Hajnsek, M. Shimada, M. Eineder, K. Papathanassiou, T. Motohka, M. Watanabe, M. Ohki, F. De Zan, P. Lopez-Dekker, G. Krieger, and A. Moreira, "Tandem-l: Science requirements and mission concept," in *EUSAR 2014; 10th European Conference on Synthetic Aperture Radar*, June 2014, pp. 1–4.
[48] N. Pierdicca, M. Davidson, M. Chini, W. Dierking, S. Djavidnia, J. Haarpaintner, G. Hajduch, G. V. Laurin, M. Lavalle, C. López-Martínez, T. Nagler, and B. Su, "The Copernicus L-band SAR mission ROSE-L (Radar Observing System for Europe) (Conference Presentation)," in *Active and Passive Microwave Remote Sensing for Environmental Monitoring III*, F. Bovenga, C. Notarnicola, N. Pierdicca, and E. Santi, Eds., vol. 11154, International Society for Optics and Photonics. SPIE, 2019. [Online]. Available: https://doi.org/10.1117/12.2534743
[49] D. Ho Tong Minh, S. Tebaldini, F. Rocca, T. Le Toan, L. Villard, and P. Dubois-Fernandez, "Capabilities of BIOMASS tomography for investigating tropical forests," *Geoscience and Remote Sensing, IEEE Transactions on*, vol. 53, no. 2, pp. 965–975, Feb 2015.
[50] S. Quegan, T. Le Toan, J. Chave, J. Dall, J.-F. Exbrayat, D. H. T. Minh, M. Lomas, M. M. D'Alessandro, P. Paillou, K. Papathanassiou, F. Rocca, S. Saatchi, K. Scipal, H. Shugart, T. L. Smallman, M. J. Soja, S. Tebaldini, L. Ulander, L. Villard, and M. Williams, "The european space agency biomass mission: Measuring forest above-ground biomass from space," *Remote Sensing of Environment*, vol. 227, pp. 44 – 60, 2019. [Online]. Available: http://www.sciencedirect.com/science/article/pii/S0034425719301233
[51] M. Crosetto, O. Monserrat, M. Cuevas-González, N. Devanthéry, and B. Crippa, "Persistent scatterer interferometry: A review," *ISPRS Journal of Photogrammetry and Remote Sensing*, vol. 115, pp. 78 – 89, 2016, theme issue 'State-of-the-art in photogrammetry, remote sensing and spatial information science'. [Online]. Available: http://www.sciencedirect.com/science/article/pii/S0924271615002415
[52] D. HO TONG MINH, Y.-N. NGO, T. T. LE, T. C. LE, H. S. BUI, Q. V. VUONG, and T. LE TOAN, "Horizontal and vertical velocities in Ho Chi Minh city by Sentinel-1 radar interferometry," Sep. 2021, This work was supported in part by the Centre National d'Etudes Spatiales/Terre, Ocean, Surfaces Continentales, Atmosphere (CNES/TOSCA - project MekongInSAR), UMR TETIS, and Institut national de recherche en agriculture, alimentation et environnement (INRAE). [Online]. Available: https://doi.org/10.5281/zenodo.5497723